BIOPHYSICS

Rhomboid-catalyzed intramembrane proteolysis requires hydrophobic matching with the surrounding lipid bilayer

Oskar Engberg[1]†, David Ulbricht[1]†, Viola Döbel[1], Verena Siebert[2,3], Christian Frie[3], Anja Penk[1], Marius K. Lemberg[2,3]*, Daniel Huster[1]*

Membrane thinning by rhomboid proteins has been proposed to reduce hydrophobic mismatch, providing a unique environment for important functions ranging from intramembrane proteolysis to retrotranslocation in protein degradation. We show by in vitro reconstitution and solid-state nuclear magnetic resonance that the lipid environment of the *Escherichia coli* rhomboid protease GlpG influences its activity with an optimal hydrophobic membrane thickness between 24 and 26 Å. While phosphatidylcholine membranes are only negligibly altered by GlpG, in an *E. coli*–relevant lipid mix of phosphatidylethanolamine and phosphatidylglycerol, a thinning by 1.1 Å per leaflet is observed. Protease activity is strongly correlated with membrane thickness and shows no lipid headgroup specificity. We infer from these results that, by adjusting the thickness of specific membrane domains, membrane proteins shape the bilayer for their specific needs.

INTRODUCTION

The lipid membrane provides the environment for membrane proteins carrying out essential cellular functions. In biological membranes, hundreds of different lipid species can modulate protein function by lateral heterogeneities in their distribution, by their spontaneous curvature, and via specific interactions with individual proteins (*1*). However, only little is known mechanistically how lipids tune protein function (*2*). Bovine rhodopsin, for instance, requires highly elastic membranes composed of polyunsaturated lipids with negative spontaneous curvature for optimal function (*3*, *4*) and shows headgroup specificity for phosphatidylethanolamine (PE) (*5*). The question of how lipids modulate the activity of membrane proteins is also key for understanding intramembrane proteolysis, an enzymatic reaction highly relevant for numerous important biological functions and pathological conditions (*6*). The membrane environment imposes a number of specific constraints and requires adaptations to enable efficient hydrolytic reaction. Compared to the aqueous environment, membrane viscosity is much higher, slowing down substrate diffusion (*7*, *8*). To overcome this problem, it has been suggested that rhomboid proteases thin their surrounding lipid annulus to break the viscosity limit of membrane protein diffusion (*9*). Moreover, rhomboid-induced membrane thinning has been suggested to influence recognition and unwinding of the helical substrate transmembrane domains (*10*). Relevance of this membrane perturbation is highlighted by the role of catalytically inactive rhomboid family proteins, so-called pseudoproteases, in other important membrane-based processes ranging from protein degradation to signaling (*11*). Likewise, the yeast rhomboid pseudoprotease Der1 has been implicated in shaping of a membrane-thinned region that facilitates retrotranslocation of protein from the endoplasmic reticulum toward proteasomal degradation (*12*). While biochemical analysis of the *Escherichia coli* rhomboid protease GlpG indicates that intramembrane proteolysis critically depends on membrane composition in vitro (*13*), its membrane thinning function has, so far, not been experimentally validated, and it is unclear how lipids modulate the conformation and activity of rhomboid proteins in general.

The concept of hydrophobic matching describes the interface between an integral membrane protein and its surrounding lipid belt (*14*, *15*). A mismatch between the hydrophobic thickness of the protein and the surrounding membrane results in unfavorable free energy that can be relieved by several mechanisms (*14*, *16*): (i) The surrounding lipids can adjust their chain order to increase or decrease acyl chain length to match the thickness of the protein, (ii) the protein can tilt or adjust its α-helical content to respond to the thickness difference of the surrounding membrane, and/or (iii) proteins can cluster to minimize the interaction with a mismatched lipid bilayer. Furthermore, membrane charge and the degree of lipid chain unsaturation influence protein-lipid interactions (*17*). For GlpG, molecular dynamics (MD) simulations have suggested that the rhomboid fold thins lipid double layers of varying composition by up to 4 Å (*10*). However, experimental data on this important subject are not available.

Here, we report measurement of the exact alteration in membrane hydrophobic thickness induced by GlpG in model membranes of varying chain lengths and headgroup compositions and relate the membrane alteration to GlpG function in the specific lipid environment. A picture emerges that GlpG function is not related to specific lipid species but requires an optimal hydrophobic thickness for most efficient substrate cleavage, which, for physiological *E. coli* membranes, can be adjusted to the optimal spacing by the rhomboid fold.

[1]Institute for Medical Physics and Biophysics, University of Leipzig, Härtelstr. 16/18, D-04107 Leipzig, Germany. [2]Center for Molecular Biology of Heidelberg University (ZMBH), Im Neuenheimer Feld 282, D-69120 Heidelberg, Germany. [3]Center for Biochemistry and Cologne Excellence Cluster on Cellular Stress Responses in Aging-Associated Diseases (CECAD), Medical Faculty, University of Cologne, Joseph-Stelzmann-Str. 52, D-50931 Cologne, Germany.
*Corresponding author. Email: daniel.huster@medizin.uni-leipzig.de (D.H.); m.lemberg@uni-koeln.de (M.K.L.)
†These authors contributed equally to this work as co–first authors.

RESULTS

GlpG only marginally influences the hydrophobic thickness of synthetic phosphatidylcholine membranes

To systematically quantify lipid distortion effects of the rhomboid fold, we reconstituted GlpG [expressed in *E. coli* as described in (*13*, *18*)] into three fully saturated phosphatidylcholine (PC) model membranes with varying acyl chain lengths (L_C), i.e., dilauroylphosphocholine (DLPC; C12:0, L_C = 9.6 Å), dimyristoylphosphocholine (DMPC; C14:0, L_C = 11.8 Å), and dipalmitoylphosphocholine (DPPC; C16:0)/cholesterol [2:1 (mol/mol)] (L_C = 17.9 Å), where cholesterol increases the DPPC chain length. The lipids were perdeuterated in their acyl chains. For each system, we measured stationary ^{2}H solid-state nuclear magnetic resonance (NMR) spectra for (i) pure lipid membranes in the absence of GlpG at pH 4 and 7, (ii) lipid membranes in the presence of GlpG at pH 4 and 7, (iii) lipid membranes in the presence of GlpG and the GlpG model substrate LacYTM2 (*19*) at pH 4, and (iv) membranes in the presence of the GlpG substrate LacYTM2 only (pH 4). At pH 4, the substrate is bound to GlpG but not cleaved as GlpG is inactive at low pH (*8*). Reconstitution of *n*-dodecyl-β-D-maltoside (DDM)–solubilized GlpG into lipid membranes was carried out using a protein-to-lipid molar ratio of 1:100 by means of the detergent 1,2-diheptanoyl-*sn*-glycero-3-phosphocholine (DHPC) (*20*). Stationary ^{2}H NMR spectra of all samples were acquired (fig. S1 and table S1), and from these spectra, the projected length of the lipid chains (L_C) was determined to a precision of ±0.1 Å using the mean torque model (*21*). L_C for the three membrane systems in the absence and in the presence of GlpG and the substrate LacYTM2 are shown in Fig. 1 (A to C).

Whereas in DLPC membrane incorporation of GlpG led to a small increase in acyl chain length (Fig. 1A), in DMPC (Fig. 1B), and DPPC/cholesterol [2:1 (mol/mol)] bilayers (Fig. 1C) within experimental error, no lipid chain length alteration by GlpG was observed. These results show that GlpG has the potential to alter very thin membranes, but, different to previous MD simulations (*10*), our experimental validation revealed a limited capacity to modulate bilayer dimensions. While these systematic alterations in membrane thickness help understand the basic interaction of GlpG with the surrounding bilayer, saturated lipids are of limited physiological relevance. Biological membranes mostly consist of phospholipids with 16 to 18 carbons with saturated *sn*-1 and unsaturated *sn*-2 chains (*22*). Therefore, we next reconstituted GlpG into physiologically relevant monounsaturated palmitoyloleoylphosphocholine (POPC; perdeuterated in the *sn*-1 chain) membranes featuring similar dimensions (L_C = 12.2 Å) as DMPC (L_C = 11.8 Å). Again, no substantial alteration in chain length is induced by GlpG (Fig. 1D).

GlpG tightly associates with PE and phosphatidylglycerol

Quantitative interpretation of the ^{2}H NMR data depends on (i) the knowledge of the exact protein-to-lipid ratio after reconstitution and requires (ii) the absence of the remaining detergent used in reconstitution. Using extensive lipid analytics, we precisely determined the protein-to-lipid ratio in all samples from quantitative thin-layer chromatography (TLC) and protein concentration measurements. Figure S2 reports all GlpG-to-lipid molar ratios of the individual samples. Almost all preparations yielded GlpG-to-lipid ratios between 1:60 and 1:130; only for the DPPC/cholesterol membranes, this ratio was lower (around 1:250). ^{1}H and ^{31}P solution NMR (Fig. 1E and figs. S3 and S4) demonstrate that no traces of DDM and DHPC (used for GlpG solubilization and reconstitution) remain in the membrane preparations. However, the ^{31}P NMR spectra revealed additional signals; one is assigned to small amounts of lyso-PC often found in synthetic lipid preparations (Fig. 1E). Furthermore, we detect two prominent signals with chemical shifts characteristic for PE and phosphatidylglycerol (PG) (*22*). Neither of these lipids was used during reconstitution, but both represent predominant species of *E. coli* membranes (*23*). It is likely that they were copurified from the *E. coli* membranes during GlpG extraction. A ^{31}P NMR spectrum of recombinant GlpG in DDM, which should not show any signals from phospholipids, detects strong PE/PG peaks (Fig. 1E). To verify the assignment, we separated the lipids by TLC and performed electrospray ionization mass spectrometry (ESI-MS) to unequivocally identify PE and PG with chain compositions typical of *E. coli* membranes (Fig. 1F and fig. S5).

PE/PG are not specific determinants of GlpG catalytic activity

On the basis of these experimental observations, we asked whether PE/PG could represent cofactors for GlpG function. To this end, we expressed completely PE/PG-free GlpG by cell-free synthesis using an *E. coli* extract in the absence of intact plasma membranes (*24*) yielding 1.2 to 1.5 mg of pure protein per milliliter extract (Fig. 2A) and solubilized it in DDM. To compare the proteolytic function of cell-free GlpG and GlpG produced in *E. coli*, a cleavage assay developed for transmembrane substrates of GlpG (*25*) was used. A variant of the substrate LacYTM2 was synthesized with DABCYL (4-((4-(dimethylamino)phenyl)azo)benzoic acid)-quenched EDANS (5-((2-aminoethyl)amino)naphthalene-1-sulfonic acid) fluorophores conjugated to either side of the cleavage site. Comparing the activity of cell-free and recombinant GlpG, represented by the initial slope in the EDANS fluorescence increase upon substrate addition, indicates higher activity of the cell-free GlpG compared to GlpG produced in *E. coli* (Fig. 2B). However, TLC analysis revealed that the cell-free produced GlpG still contained PE and PG (Fig. 2C), which are present in the cell-free *E. coli* extract as confirmed by TLC (Fig. 2D). To remove these PE/PG lipids, we applied a protocol optimized for the refolding G protein–coupled receptors (*20*) to reconstitute GlpG into DMPC membranes involving SDS solubilization, metal chelate affinity chromatography, and subsequent extraction of detergent using biobeads. This procedure lastly resulted in a GlpG preparation that was completely free of PE/PG (Fig. 2, D and E). This preparation showed high proteolytic activity in DMPC membranes (Fig. 2F), demonstrating that neither PE nor PG is required for GlpG-catalyzed intramembrane proteolysis.

E. coli lipids modulate GlpG activity

After establishing that reconstituted GlpG is fully functional in the absence of PE/PG, we asked what the role of these tightly bound lipids is. To this end, we reconstituted cell-free produced PE/PG-free GlpG into DMPC membranes, which were substituted with small concentrations of the *E. coli* lipids PE and PG [1 to 20 mole percent (mol %) of a 75/25 mix of palmitoyloleoylphosphatidylethanolamine (POPE)/POPG (1-palmitoyl-2-oleoyl-sn-glycero-3-phospho-(1′-rac-glycerol)] and carried out cleavage assays (Fig. 2G). The activity of GlpG in DMPC membranes, represented by the initial slope in the EDANS fluorescence increase upon cleavage, was set to 100% as the reference point. Consistent with a previous analysis (*13*), even a small concentration of 1 mol % PE/PG already reduced the velocity of LacYTM2 cleavage by GlpG to 34%, and in the presence of 20 mol % PE/PG, GlpG cleavage velocity is reduced to 16%. This result suggests that

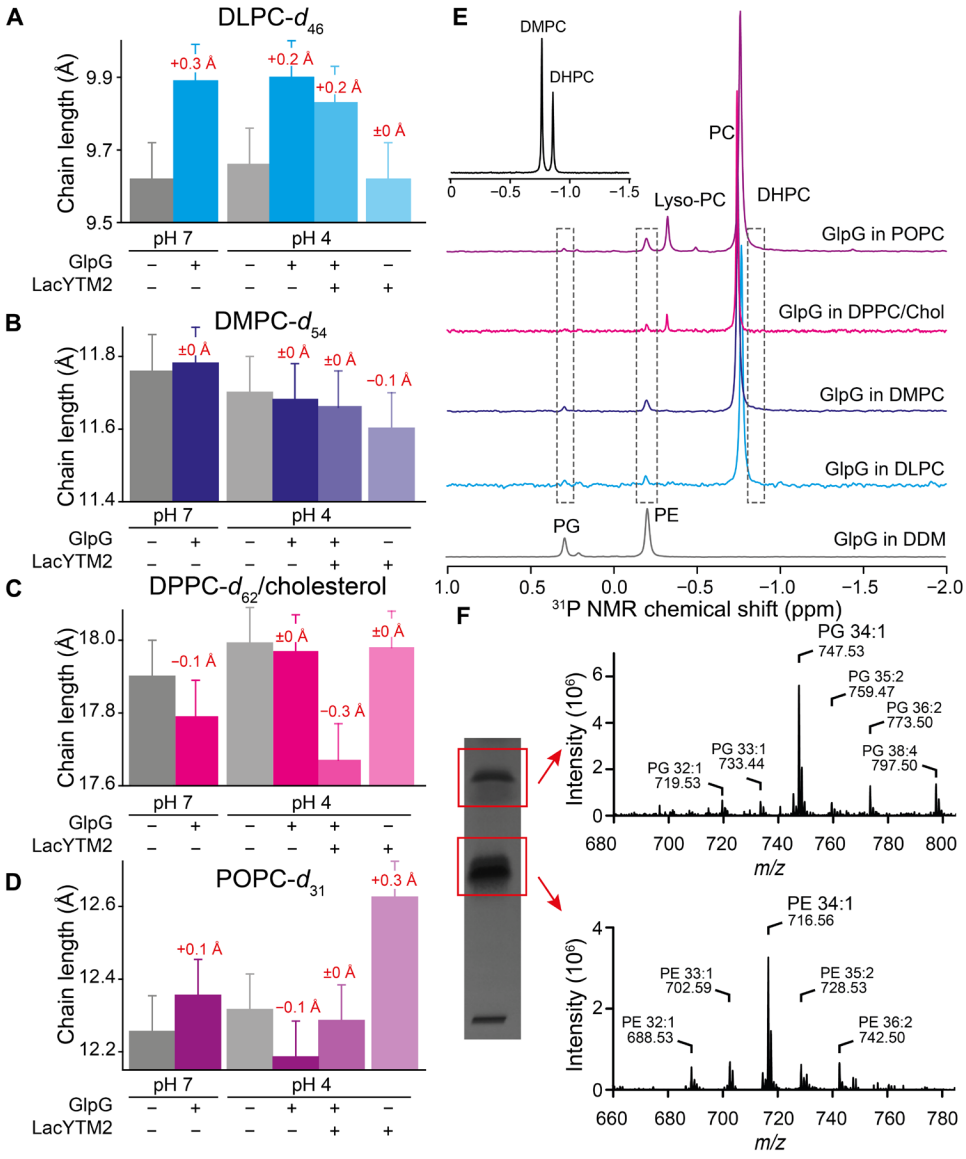

Fig. 1. Influence of GlpG on lipid chain lengths in PC membranes and lipid analytics. (**A** to **D**) Average acyl chain length of (A) DLPC, (B) DMPC, (C) DPPC/cholesterol [2:1 (mol/mol)], and (D) POPC membranes in the absence (gray bars) and in the presence of GlpG and the GlpG substrate LacYTM2 (colored bars) at pH 7 and 4. Error bars represent ±0.1 Å (*21*), and -d_x denotes the number of deuterons in the lipid chains. (**E**) ^{31}P NMR spectra of all GlpG/membrane preparations solubilized in cholate. No remaining DHPC (inset shows a reference spectrum of DHPC/DMPC) was detected in either preparation. Downfield signals are assigned to PE and phosphatidylglycerol (PG) also present in DDM-solubilized GlpG. In (**F**), the thin-layer chromatogram is shown along with the ESI mass spectra of the TLC spots confirming the presence of PE and PG in the reconstituted samples. ppm, parts per million; *m/z*, mass/charge ratio.

E. coli lipids exert an inhibitory effect on GlpG, and the in vitro assay with PE/PG-free GlpG has the capacity to unleash a higher activity as in the native membrane.

Physiological interaction with PE/PG triggers GlpG-mediated membrane thinning

While GlpG is fully active in the absence of *E. coli* lipids, it remains intriguing that PE/PG lipids inhibit GlpG activity. Therefore, we investigated whether reconstitution of GlpG into an *E. coli*–relevant lipid mix had any impact on PE/PG membrane properties. To this end, we reconstituted GlpG into an *E. coli*–like 3:1 (mol/mol) POPE/POPG mixture (*23*) with deuterium labeling on either of the palmitoyl chains and measured lipid chain lengths in these membranes. In contrast to the various PC membranes (Fig. 1), the presence of GlpG leads to a pronounced thinning of ≥1.0 Å per membrane leaflet for both POPE and POPG (Fig. 3, A and B). This suggests a specific interaction of GlpG with either lipid, leading to a conformational change in the lipid annulus around GlpG as the cause for the membrane thinning. The decrease in chain length is caused by the introduction of one additional gauche defect into the chain for both POPE and POPG, leading to an increase in area per molecule by ~4 to 7 Å^2 as calculated from the ^{2}H NMR spectra using previously published models (table S1) (*21*). To check whether the pronounced thinning of POPE/POPG membranes by GlpG was a

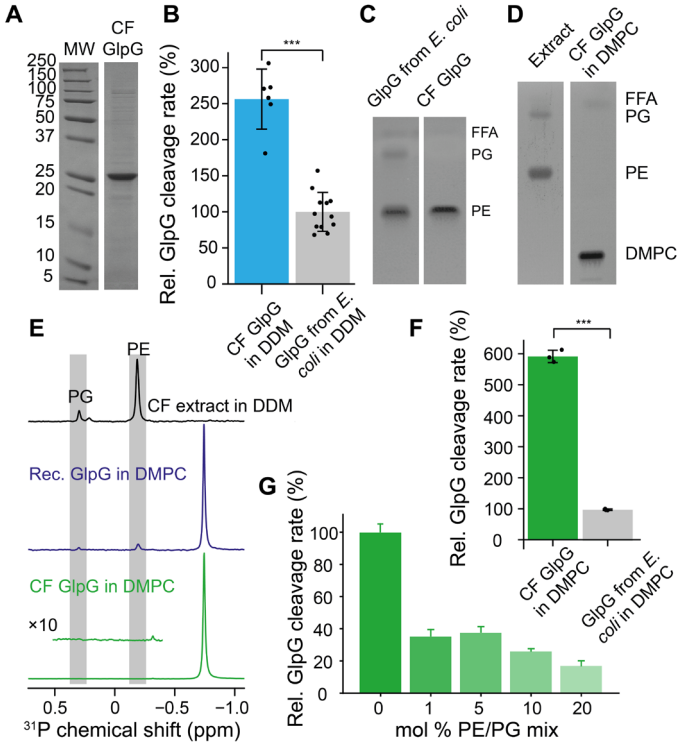

Fig. 2. Lipid binding and functionality assay of cell-free expressed GlpG. (**A**) Coomassie-stained gel showing the purity of cell-free (CF) expressed GlpG. MW, molecular weight. (**B**) Comparison of the cleavage rate of *E. coli*–expressed GlpG (set to 100% as reference) and cell-free GlpG reported as the initial slope in the fluorescence signal of the EDANS signal of LacYTM2. GlpG was solubilized in DDM (0.05%), and LacYTM2 was added in dimethyl sulfoxide (0.5%). (**C**) TLC results for both samples showing the presence of PE and PG. FFA, free fatty acids. Only cell-free GlpG, reconstituted into DMPC membranes, is completely free of PE and PG as shown in (**D**) TLC analysis and (**E**) ^{31}P NMR spectroscopy. Rec, recombinantly expressed in *E. coli*. (**F**) Activity of cell-free GlpG compared to *E. coli*–produced protein. (**G**) Relative cleavage rate of cell-free GlpG reconstituted into DMPC membranes (set to 100%) as a function of increasing concentrations of POPE/POPG (at a 75/25 mixing ratio). Cleavage assays were carried out at pH 7. Significances were determined using Welch two-sample two-tailed *t* test (***$P < 0.001$).

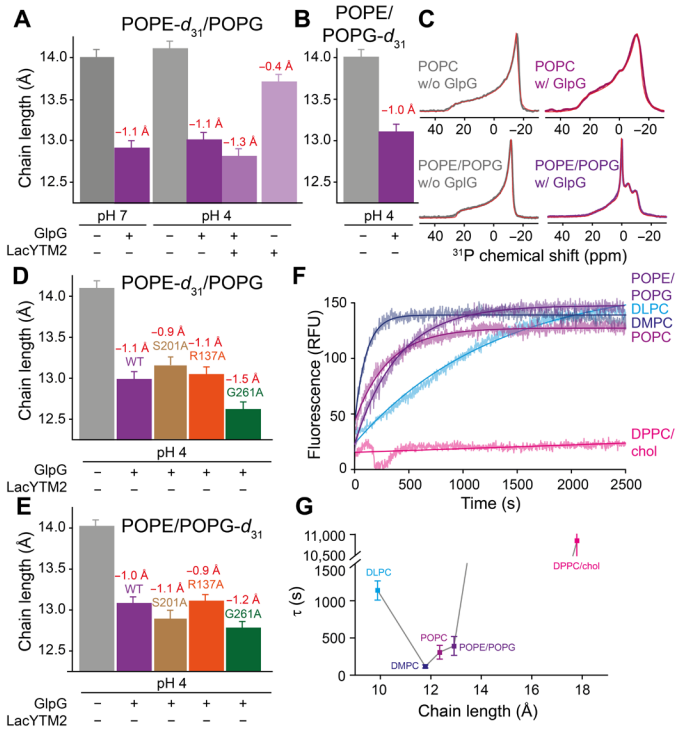

Fig. 3. Influence of GlpG on lipid chain lengths in PE/PG membranes and GlpG activity. Average acyl chain length of (**A**) POPE and (**B**) POPG in mixed membranes of POPE/POPG [3:1 (mol/mol)] in the absence (gray bars) and in the presence of GlpG and the LacYTM2 substrate (colored bars). (**C**) Stationary ^{31}P NMR spectra of POPC (top) and POPE/POPG membranes (bottom) in the absence and presence of GlpG. (**D** and **E**) Influence of the GlpG mutations S201A, R137A, and G261A on the chain length of (D) POPE and (E) POPG. WT, wild type. (**F**) Time course of EDANS fluorescence intensity increase of cleaved LacYTM2 induced by activation of GlpG by a pH jump from 4 to 7. RFU, relative fluorescence units. (**G**) Characteristic GlpG cleavage time constant (τ) versus lipid membrane chain length.

consequence of the negatively charged POPG, we also investigated POPC/POPG [3:1 (mol/mol)] membranes in the absence and in the presence of GlpG. No substantial thinning was observed in these membranes (fig. S6), suggesting that the negative charge of POPG is not the decisive factor in the specific thinning of POPE/POPG membranes.

This specific interaction between GlpG and POPE/POPG was confirmed by stationary solid-state ^{31}P NMR measurements (Fig. 3C and fig. S7). In the absence of GlpG, all membrane samples showed the well-known ^{31}P NMR powder pattern indicative of lipids in planar membranes undergoing axially symmetric rotational diffusion (*22*). Addition of GlpG to POPC membranes only slightly broadens the NMR spectra, while the chemical shift anisotropy (Δσ) was slightly decreased from 45 to 41 parts per million (ppm). In contrast, the ^{31}P NMR spectra of the POPE/POPG membranes drastically change upon addition of GlpG. In the absence of GlpG, the ^{31}P NMR spectrum is characterized by a single axially symmetric contribution with Δσ = 37 ppm, which decreased to 31 ppm in the presence of the protease. An additional anisotropic contribution (Δσ = 16 ppm) and an isotropic signal are detected in the GlpG-containing sample. These additional spectral features account for 26 and 18% of the intensity, respectively, and indicate lipid molecules with altered headgroup orientation and dynamics (*26*, *27*). These additional spectral features were not observed in the POPC/POPG mixtures (fig. S6), suggesting that, particularly, POPE interacts with GlpG presumably by hydrogen bond formation.

We conducted a number of control experiments to confirm that the characteristic changes in the ^{31}P NMR spectra truly indicate specific interaction of GlpG with PE/PG headgroups. First, we measured the size distribution of the POPE/POPG membrane samples in the absence and in the presence of GlpG. Vesicle size changes induced by the protein could lead to additional averaging resulting in the spectral features observed in the ^{31}P NMR spectra. To rule out that GlpG induces formation of a highly curved lipid structure, we measured the size distribution of the POPE/POPG multilamellar vesicles (MLVs) using dynamic light scattering (fig. S8). In the absence of GlpG, a rather homogeneous size distribution with vesicle diameters between 420 and 580 nm is observed. In the presence of GlpG, vesicle size increases, showing a broader distribution with a maximum between 1410 and 1640 nm. From these results, we can exclude that GlpG induces formation of small vesicles that would lead to the observed additional signals in the ^{31}P NMR spectra of POPE/POPG membranes in the presence of GlpG.

Second, as lyso-lipids were observed in some preparations, we investigated whether these single-chain lipids could be causative for the additionally detected isotropic and anisotropic contributions in the stationary ^{31}P NMR spectra. To confirm that these alterations were not caused by lyso-PE, we carried out control experiments of POPE/POPG membranes in the presence of increasing concentrations of lyso-PE (7 to 38 mol %). Although a small decrease in $\Delta\sigma$ was observed with increasing lyso-PE concentration (fig. S9), we found neither isotropic contributions nor anisotropic contributions with much reduced $\Delta\sigma$. All these control measurements strongly support our conclusion that the additional features observed in the ^{31}P NMR spectra indicate specific interactions of GlpG with the lipid headgroups leading to altered headgroup orientation and dynamics. These features are not caused by lipid molecules in small vesicles with high curvature or isotropic lipid phases. If highly curved lipid structures were present in our preparations, then we would also have detected these spectral features in the ^{2}H NMR spectra of the same samples, which was not the case. All this supports the conclusion that these features in the ^{31}P NMR spectra indicate alterations in headgroup orientation/dynamics induced by GlpG interaction.

The influence of GlpG on phospholipid headgroup dynamics was also observed in ^{31}P magic angle spinning (MAS) NMR spectra shown in fig. S10. Under MAS conditions, solution-like NMR spectra without any anisotropic contributions are detected (*22*). Most obviously, addition of GlpG leads to a broadening of the ^{31}P MAS NMR signals. This is least pronounced in POPC membranes, stronger in POPC/POPG mixtures, and very obvious in POPE/POPG mixtures, where the ^{31}P MAS NMR signal is severely broadened. We also measured T_1 and T_2 relaxation times (fig. S10) for these membrane preparation. While moderate alterations in T_1 were observed in the presence of GlpG in all lipid samples, T_2 relaxation times, which are also sensitive to slower motions, strongly decreased in the presence of GlpG. The most pronounced decrease of more than 90% was observed for POPE/POPG membranes because of the presence of GlpG indicating alterations in lipid headgroup dynamics due to protein interaction.

Because GlpG causes prominent thinning of POPE/POPG membranes, we asked whether the catalytic activity of GlpG relates to POPE/POPG membrane thinning. The GlpG S201A active site mutant shows a similar reduction of POPE/POPG chain lengths (Fig. 3, D and E, and fig. S11), indicating that membrane thinning of *E. coli*–like membranes is also induced by catalytically dead GlpG. Consistent results were observed for other inactive GlpG variants, namely, the R137A mutation in the characteristic membrane-embedded loop 1 or mutation of an invariant GxxxG motif in transmembrane helix 6 (G261A). This suggests that thinning of *E. coli*–like membranes is caused by the tertiary structure of the rhomboid fold and specific interactions between GlpG residues with PE/PG headgroups are at least not directly related to the enzyme reaction cycle.

The membrane thickness determines the velocity of GlpG-catalyzed cleavage

To investigate GlpG activity in different membranes, we modified the aforementioned cleavage assay for better quantification. Samples of co-reconstituted GlpG and LacYTM2 were prepared at pH 4, where GlpG is inactive and no EDANS fluorescence of LacYTM2 is detected. A pH jump to 7 activates GlpG, and cleavage of LacYTM2 is monitored by increasing EDANS fluorescence over time. Fluorescence intensity was fitted by a single exponent [$I(t) = I_{max} - I_0 \cdot \exp.(-t/\tau)$], providing a characteristic time constant τ that describes the velocity of substrate turnover (Fig. 3F and table S2). Fastest substrate processing is detected in DMPC (τ = 117 ± 17 s) followed by POPC (τ = 309 ± 92 s) and POPE/POPG membranes (τ = 393 ± 126 s). LacYTM2 cleavage by GlpG is much slower in DLPC membranes (τ = 1139 ± 129 s) and is almost completely abolished in the DPPC/cholesterol mixture (τ = 10,835 ± 4298 s). However, the TAMRA probe activity assay still shows the structural integrity of GlpG in DPPC/cholesterol membranes (fig. S12). A plot of the characteristic time of LacYTM2 cleavage in different membrane environments versus lipid chain length reveals an optimum for efficient proteolytic activity for lipid membranes with an average chain length of ~12 to 13 Å (Fig. 3F). This provides direct biophysical evidence that the dimension of the surrounding lipid bilayer represents a decisive factor for the enzymatic activity of GlpG irrespective of specific properties of the phospholipids.

DISCUSSION

The huge lipid variety in cells from various tissues of all organisms remains enigmatic and gives rise to speculation about its biological importance (*1*). However, examples for specific and functionally relevant lipid-protein interaction are rare to this point (*2*, *28*). Here, we describe how a rhomboid family protein actively influences the hydrophobic thickness of the surrounding membrane of a specific composition but leaves other lipid environments completely unperturbed. The picture emerges that the GlpG function is correlated with the membrane's hydrophobic thickness, which the protein can actively influence as summarized in Fig. 4.

The window of optimal membrane thickness for GlpG function is ~12 to 13 Å (Fig. 3G) per leaflet as found in DMPC or POPC bilayers, where the structure of GlpG minimizes energetically costly perturbations. This corresponds well to the hydrophobic thickness of GlpG of 27 Å (corresponding to 13.5 Å per membrane leaflet) reported in the crystal structure (*29*). Pure POPE/POPG bilayers representing a good model of the *E. coli* membranes (*23*) show more extended acyl chains (L_C = 14.0 Å) than POPC (L_C = 12.2 Å) despite their identical chain composition due to negative intrinsic curvature of PE (*3*, *5*). For optimal function, GlpG actively thins POPE/POPG membranes by 1.1 Å per leaflet shown experimentally in this study. In the presence of GlpG, the differences in POPC versus POPE/POPG membrane thickness almost completely vanish (L_C = 12.4 Å versus L_C = 12.9 Å). Such membrane thinning requires specific interaction of GlpG with PE/PG lipids to relax curvature pressure directly seen in the ^{31}P solid-state NMR spectra, where altered headgroup structure and dynamics are observed, linewidths increase, and NMR relaxation times are strongly influenced (Fig. 3C and fig. S10), suggesting an "energetic coupling" (*30*) between GlpG and PE/PG headgroups. Specific interactions between GlpG and PE/PG headgroups lead to different headgroup orientation as seen in the ^{31}P NMR spectra, but the general bilayer structure remains intact, although with decreased lipid chain order leading to membrane thinning. The influence of GlpG on PE/PG headgroup orientation and dynamics is an example of how a membrane protein actively influences its lipid annulus. It should be noted that *E. coli* lipids also contain molecules with branched chains or chains with cyclocarbons. While we here focus on headgroup specificity and hydrophobic matching, the differences in the chain composition of the synthetic lipid mix used here and the native *E. coli* composition may give rise to additional effects.

This active lipid-protein interaction has important functional consequences. We show that GlpG activity is primarily related to

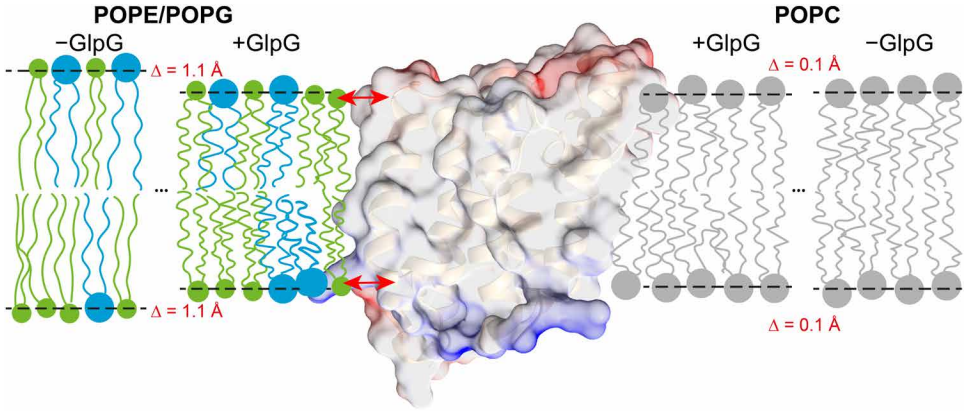

Fig. 4. Model of GlpG-induced membrane thinning. GlpG specifically interacts with PE/PG lipids (shown in green and blue, respectively) to thin the bilayer at the protein/membrane interface by 1.1 Å per lipid leaflet (left). In contrast, the hydrophobic thickness of a POPC membrane (shown in gray on the right) is not influenced by GlpG as the free-standing POPC bilayer already provides the optimal membrane environment for GlpG. Arrows indicate putative interactions of PE/PG headgroups with GlpG. GlpG [Protein Data Bank, code 2IC8 (*29*)] is shown as surface representation with blue and red color for positive and negative surface charges, respectively.

membrane thickness, also reported for γ-secretase, another important intramembrane protease (*31*). At the same time, the lipid headgroup chemistry may have a modulatory effect, too. Unexpectedly, the fastest enzyme reaction is observed in pure DMPC membranes, which are completely artificial and have no relevance for *E. coli*. Under these circumstances, *E. coli* lipids even inhibit GlpG function (Fig. 2G). To a limited extent, the rhomboid tolerates non-natural lipid headgroups and acyl chains, as well as a variety of membrane thicknesses. Nonetheless, optimal hydrophobic matching remains the crucial determinant for GlpG function, and increasing hydrophobic mismatch between protein and membrane environment reduces cleavage velocity. The building block of the rhomboid fold is a bundle of six transmembrane helices with the catalytic serine (S201) positioned at the top of the central, tilted shorter helix forming a membrane-embedded active site cavity with a lateral substrate gate and a capped opening to the periplasmic space (*29*). Another prominent structural feature of the rhomboid fold is loop 1 that extends sidewise into the periplasmic leaflet of the lipid bilayer, with the highly conserved tryptophan-arginine motif snorkeling out of the hydrophobic membrane core. Inactive GlpG mutants including the S201A active site mutation, which are predicted to have the same three-dimensional structure, induce the same thinning of PE/PG bilayers. While our activity profiling of reconstituted GlpG shows that the membrane dimension is the critical determinant for rhomboid activity, the observation that the active site serine (S201) is dispensable for membrane thinning indicates that the lipid bilayer and the observed membrane immersion do not directly participate in formation of the proteolytic scission complex. Instead, we may speculate that the membrane geometry affects substrate recognition by a putative rhomboid exosite (*32*). The GxxxG motif in the center of the rhomboid fold, which is essential for the function of rhomboid proteases and pseudoproteases (*33*, *34*), also does not affect membrane thinning, indicating that features on the surface are responsible for the effect (Fig. 4). Whereas mutation of the conserved R137 in loop 1, which previously had been suggested by MD simulation to form a strong hydrogen bond to the headgroups of POPE (*35*), does not notably contribute to thinning, we suggest that other surface-exposed GlpG side chains may form hydrogen bonds to the PE/PG but not to PC. Therefore, GlpG is much less efficient in altering the thickness of PC membranes. The gain in free energy from hydrogen bond formation with PE/PG headgroups is used to compress the lipid chains to produce the observed thinning. Which structural features of the conserved rhomboid fold govern these specific interactions remains an important question. As the control samples of POPC/POPG did not show a GlpG-induced thinning (fig. S6), electrostatic interactions only do not seem to play the decisive role.

The biological implication from these results is that the lipid environment can fine-tune membrane protein function. Vice versa, a membrane protein can also shape the bilayer to its specific needs. It is known that membrane lateral organization is spatially and temporally heterogeneous, leading to transient domains, which vary in their hydrophobic thickness (*1*). Thus, by dynamic domain formation, orchestrated by specific integral membrane proteins, cells can locally adjust bilayer thickness and thus enable a plethora of different biological activities. How may membrane thickness be coupled to function? It is attractive to speculate an interplay between the membrane hydrophobic thickness and the three-dimensional arrangement of the α helices forming GlpG's lateral active site gate thereby modulating substrate access and cleavage velocity. This reflects the structural plasticity of α-helical membrane proteins and their importance for biological function.

Evolution has optimized the composition of biological membranes to the degree of lateral and transversal lipid heterogeneity (*1*). This environment provides the best compromise for optimal function of all embedded proteins. Our data show that the surrounding membrane directly influences the activity of GlpG, which, along with specific lipid-protein interactions, provides a means to enable protein function within cellular membranes. In general, the rhomboid fold emerges as an evolutionarily conserved module, which, not only in the context of active intramembrane proteases but also as pseudoprotease, determines the fate of membrane proteins. Distortion of the lipid bilayer and membrane thinning emerges a general principle underlying a wide range of biologically important processes ranging from protein translocation (*36*) to substrate selection of membrane-anchored proteases (*37*).

MATERIALS AND METHODS

For detailed experimental procedures, see the Supplementary Materials.

Materials

LacYTM2 peptides were custom synthesized by the Core Unit Peptide Technologies at the University of Leipzig, Germany. All lipids were purchased from Avanti Polar Lipids (Alabaster, AL). DDM was bought from Glycon (Luckenwalde, Germany). All other chemicals were purchased from Sigma-Aldrich (Taufkirchen, Germany).

Recombinant expression of GlpG

The sequence of the *E. coli* GlpG wild type (WT) (UniProt, ID P09391) was cloned into *E. coli* expression vector pET-25b(+) (Novagen) with a C-terminal hexahistidine-tag (GlpG-His_6). Single mutations (S201A, R137A, or G261A) in the GlpG sequence were introduced by site-directed mutagenesis according to Stratagene's QuikChange protocol (Agilent Technologies, Santa Clara, CA, USA). The expression vector was transformed into chemically competent BL21(DE3)pLysS cells (Novagen), grown in LB medium (Miller) containing ampicillin (100 μg/ml) and chloramphenicol (34 μg/ml) at 37°C. Expression of the protein in *E. coli* and purification were done as described earlier (*13*, *18*). For cell-free expression, the GlpG WT sequence was cloned from the pET-25b(+) (Novagen) plasmid into the pIVEX2.3d plasmid (Biotechrabbit GmbH, Hennigsdorf, Germany) using PIPE (Polymerase Incomplete Primer Extension) cloning (*38*). Cell-free expression of Ser-GlpG-His6 was performed as previously described with the following specifications (*39*): The cell-free reaction was performed with an 18 mM Mg^{2+} concentration and for 24 hours at 34°C in a total volume of 2 ml. The precipitated GlpG was pelleted by centrifugation (10,000*g*, 10 min, 20°C) and was washed three times with a 50 mM tris and 150 mM NaCl (pH 7) buffer. Subsequently, GlpG was solubilized in 1.5% DDM in a 50 mM tris and 150 mM NaCl (pH 7) buffer for 3 hours at room temperature on a rotating wheel. Solubilized protein was then separated from insoluble protein using centrifugation (10,000*g*, 15 min, 20°C) and was lastly applied to IMAC (Immobilized Metal Chelate Affinity Chromatography) purification using an Äkta purifier system (GE Healthcare, Chicago, USA). In the second approach, solubilization in SDS, purification, and reconstitution were performed as described (*39*) with slide adaptations. Briefly, 18 ml of 50 mM sodium phosphate, 15 mM SDS, and 50 mM dithiothreitol (pH 6.5) were added to the cell-free reaction mix and were dialyzed for 24 hours against 50 mM sodium phosphate and 15 mM SDS (pH 6.5) for the solubilization of the GlpG protein. Subsequently, the solution was adjusted to pH 8 and applied to IMAC purification using an Äkta purifier system and a HisTrap column (both from GE Healthcare, Chicago, USA). Elution was performed by a pH shift to 4.5. Last, the purified GlpG was dialyzed for 60 hours against 50 mM sodium phosphate, 15 mM SDS, and 1 mM EDTA (pH 8.9) to reduce the SDS concentration before reconstitution of GlpG into DMPC membranes as described below.

Reconstitution of GlpG into lipid membranes

The respective lipids dispersed in either pH 7 buffer (50 mM tris and 150 mM NaCl) or pH 4 buffer (50 mM sodium acetate and 150 mM NaCl) were extruded through two stacked 100-nm polycarbonate filters to produce large unilamellar vesicles using the lipid extruder (Lipex Biomembranes, Vancouver, BC, Canada) as described in the literature (*40*). DHPC was added to produce bicelles, at molar detergent:lipid excess ratio of four- to sixfold. For substrate-containing samples, LacYTM2 was added in a substrate/GlpG molar ratio of 1.2 at the same time as DHPC addition. *E. coli*–produced GlpG (in DDM) was added, either adjusted to pH 4 or in elution buffer [50 mM Hepes, 300 mM NaCl, 10% (v/v) glycerol, 400 mM imidazole, and 0.05% DDM (pH 7.4)] to the bicelles. Cell-free GlpG was added in NaP buffer [50 mM NaP, 2 mM SDS, and 1 mM EDTA (pH 7.8)]. Samples were diluted to GlpG (0.5 to 1 mg/ml) if needed by detergent buffer at pH 4 or pH 7 that contained 0.05 weight % of DDM for protein stability. The samples were then incubated for 20 min in a 42°C water bath and 20 min on ice three times to integrate GlpG and the substrate into the bicelles. Afterward, Bio-Beads SM-2 (100 mg/ml) (Bio-Rad, CA, USA) were added to remove DHPC and DDM, and samples were gently shaken overnight at 4°C to form MLVs. The procedure was repeated if needed with fresh biobeads until the solution turned turbid, indicating the formation of MLVs. The biobeads were removed by centrifugation (20 min at 21,500*g*) through a 100-μm EASYstrainer filter (Greiner, Frickenhausen, Germany) at 4°C.

NMR spectroscopy

^{2}H NMR spectra were acquired on a Bruker 750 Avance I NMR spectrometer at a resonance frequency of 115.1 MHz. The phase-cycled quadrupolar echo sequence was used for signal acquisition (*41*). A π/2 pulse length of 2.5 to 4 μs separated by a 30-μs delay was used with a spectral width of 500 kHz and a recycle delay of 1 s. All measurements were performed at 37°C. The ^{2}H spectra were dePaked, and smoothed chain order parameters were calculated according to (*42*, *43*). Projected chain lengths were calculated using the mean-torque model (*21*). Stationary ^{31}P NMR spectra were acquired on a Bruker Avance III 600-MHz spectrometer at a resonance frequency of 242.9 MHz. Hahn echo pulse sequence was used with 10 μs of 90° pulse length and an echo delay of 50 μs, a spectral width of 50 kHz, and relaxation delay of 3 s. Low-power broadband ^{1}H decoupling ($\omega_H/2\pi$ = 2.5 kHz) was applied during acquisition. Stationary ^{31}P NMR spectra were simulated as described in (*44*). ^{31}P MAS NMR spectra were acquired on a Bruker Avance Neo 700-MHz NMR spectrometer using a double-resonance MAS probe with a 3.2-mm spinning module and a MAS frequency of 10 kHz. Typical ^{31}P 90° pulse lengths were 4 μs, and ^{1}H low-power decoupling ($\omega_H/2\pi$ = 2.1 kHz) was applied during acquisition. T_1 and T_2 relaxation times were measured using standard inversion recovery and CPMG (Carr-Purcell-Meiboom-Gill) pulse sequences, respectively.

For lipid analytics, samples were resolved in cholate [200 mM sodium cholate, 50 mM Hepes, and 5 mM EDTA in D_2O:H_2O (1:8) (pH 7.6 to 7.7)]. Standard 1D ^{1}H and ^{31}P NMR spectra were acquired on a Bruker Avance III 600-MHz instrument.

Protein and peptide quantification

The concentration of GlpG in the NMR samples was determined by resolving the MLV preparations in detergent buffer [50 mM tris, 150 mM NaCl, and 50 mM SDS (pH 7)] and subsequent absorption measurements at 280 nm at a NanoDrop 1000 spectrometer (NanoDrop Technologies, Wilmington, DE, USA). Protein concentration was calculated using the Lambert-Beer law. The concentration of the LacYTM2 peptide was determined using the Pierce BCA Protein Assay Kit (Thermo Fisher Scientific, Waltham, MA USA) according to the manufacturer's protocol and was measured at an Infinite M200 plate reader (Tecan, Männedorf, Switzerland). The concentration of the LacYTM2 (EDANS/DABCYL) kinetic peptide

variant was determined by absorption measurements of the DABCYL group at 453 nm. The final peptide concentration was then calculated from a calibration curve (linear model) recorded with the LacYTM2 (EDANS/DABCYL) peptide in dimethyl sulfoxide (DMSO).

High-performance thin-layer chromatography

Samples were resolved in pH 7 buffer (50 mM tris and 150 mM NaCl) or pH 4 buffer (50 mM sodium acetate and 150 mM NaCl). Lipid extraction was done according to Bligh and Dyer (*45*). Briefly, 100 µl of a buffer-resolved MLV sample was mixed with 200 µl of $CHCl_3$/MeOH [1:1 (v/v)] for 30 s. Subsequently, phase separation was obtained by centrifugation at 20°C and 10,000*g* for 5 min. The $CHCl_3$ phase containing the lipids was placed into a vacuum centrifuge to evaporate the organic solvent. For lipid quantification, the lipid film was resolved in $CHCl_3$ and spotted on an high-performance TLC (HPTLC) silica gel 60 plate (Merck KGaA, Darmstadt, Germany) using a CAMAG Linomat 5 sample application system (CAMAG, Berlin, Germany) in addition to a lipid calibration standard on the same HPTLC plate. TLC was developed in a glass chamber (CAMAG, Berlin, Germany) with a mobile phase for lipid separation: chloroform/ethanol/water/triethylamine [30:35:7:35 (v/v/v/v)] for either 2 to 3 hours (PC lipids) or 45 min (PE/PG lipids). Lipid spot visualization was achieved by primuline staining in 200 ml of acetone/H_2O [4:1 (v/v)] and subsequent excitation under ultraviolet light. The lipid concentration in the MLV sample was lastly calculated using the calibration curve (nonlinear model) recorded with an appropriate lipid standard.

Mass spectrometry

For lipid analysis, ESI-MS was performed after HPTLC. The lipid spots on the TLC were extracted for 45 s using a Plate Express TLC plate reader (Advion, Ithaca, NY, USA) with methanol and directly applied to an amaZon SL ESI-MS spectrometer (Bruker Daltonics GmbH, Bremen, Germany). Lipid ESI-MS was performed with the following parameters: spray voltage of 4.5 kV, end plate offset of 500 V, nebulizer gas of 7.3 psi, drying gas (N_2) of 4 liters/min, dry temperature of 180°C, flow rate of 3 µl/min, and sheath gas (He) flow rate of 25 arbitrary units (a.u.). Mass spectra were recorded using the alternating positive/negative mode including enhanced resolution. For matrix-assisted laser desorption/ionization (MALDI)–MS analysis of purified GlpG WT or mutants in DDM micelles, aliquots were desalted using C18 ZipTip Pipette Tips C_{18} (Merck KGaA, Darmstadt, Germany) according to the manufacturer's protocol. MS was performed using α-cyano-4-hydroxycinnamic acid (HCCA) matrix (Merck KGaA, Darmstadt, Germany) on an autoflex speed mass spectrometer (Bruker Daltonics GmbH, Bremen, Germany) in linear mode. For MALDI–time-of-flight–MS analysis, sample aliquots containing 100 µg of GlpG were resolved in reconstitution buffer and subjected to a Bligh and Dyer extraction (*45*). Briefly, 100 µl of a buffer-resolved MLV sample was mixed with 200 µl of $CHCl_3$/MeOH [1:1 (v/v)] for 30 s. Subsequently, phase separation was obtained by centrifugation at 20°C and 10,000*g* for 5 min. The $CHCl_3$ phase containing the lipids was carefully removed. The remaining interphase (MeOH/water) was air-dried overnight. On the next day, the air-dried protein pellet was resolved in 40 µl of 25% acetonitrile/75% methanol/1% trifluoroacetic acid. MS was performed using the HCCA matrix (Merck KGaA, Darmstadt, Germany) on the autoflex speed mass spectrometer.

Enzymatic cleavage assays

For functional studies in membranes, both GlpG and the peptide substrate LacYTM2 (EDANS/DABCYL) (molar ratio of 1:1.2) were reconstituted at pH 4, where GlpG is inactive. The fluorescence assay was performed with a GlpG concentration of 6 µM in a final volume of 50 µl at pH 7 and pH 4 at 37°C. Progress of substrate cleavage over time was monitored by measuring the EDANS fluorescence using an Infinite M200 plate reader (Tecan, Männedorf, Switzerland). Progress curves were fitted to a single exponent $I(t) = I_{max} - I_0 \cdot \exp.(-t/\tau)$, with $I(t)$ being the EDANS fluorescence signal as a function of time, I_0 being the fluorescence at time point zero (=offset), I_{max} being the maximal fluorescence, and τ being a characteristic time constant. For functional studies in DDM micelles, GlpG WT or mutants (S201A, R137A, or G261A) were incubated with the kinetic peptide substrate LacYTM2 (EDANS/DABCYL) in DDM micelles at 0.4 µM protein concentration, and substrate cleavage was monitored over time. Micelles were incubated with 10 µM LacYTM2 (EDANS/DABCYL) in buffer [20 mM Hepes, 150 mM NaCl, 0.5% (v/v) DMSO, and 0.05% DDM (pH 7.4)] in a total volume of 50 µl at 37°C. Substrate cleavage was monitored by measuring the EDANS fluorescence using the plate reader. The initial slope of the reaction was calculated from a linear regression of the measured data and was used as an indicator of GlpG protease activity.

Statistical methods

Where appropriate, a Welch two-sample two-tailed *t* test was carried out in R (version 4.1.0; R Foundation for Statistical Computing, Vienna, Austria).

SUPPLEMENTARY MATERIALS

Supplementary material for this article is available at https://science.org/doi/10.1126/sciadv.abq8303

View/request a protocol for this paper from *Bio-protocol*.

REFERENCES AND NOTES

1. E. Sezgin, I. Levental, S. Mayor, C. Eggeling, The mystery of membrane organization: Composition, regulation and roles of lipid rafts. *Nat. Rev. Mol. Cell Biol.* **18**, 361–374 (2017).
2. C. R. Sanders, J. M. Hutchison, Membrane properties that shape the evolution of membrane enzymes. *Curr. Opin. Struct. Biol.* **51**, 80–91 (2018).
3. A. V. Botelho, N. J. Gibson, R. L. Thurmond, Y. Wang, M. F. Brown, Conformational energetics of rhodopsin modulated by nonlamellar-forming lipids. *Biochemistry* **41**, 6354–6368 (2002).
4. B. J. Litman, D. C. Mitchell, A role for phospholipid polyunsaturation in modulating membrane protein function. *Lipids* **31**, S193–S197 (1996).
5. O. Soubias, W. E. Teague, K. Gawrisch, Evidence for specificity in lipid-rhodopsin interactions. *J. Biol. Chem.* **281**, 33233–33241 (2006).
6. N. Kuhnle, V. Dederer, M. K. Lemberg, Intramembrane proteolysis at a glance: from signalling to protein degradation. *J. Cell Sci.* **132**, jcs217745 (2019).
7. F. Kamp, E. Winkler, J. Trambauer, A. Ebke, R. Fluhrer, H. Steiner, Intramembrane proteolysis of β-amyloid precursor protein by γ-secretase is an unusually slow process. *Biophys. J.* **108**, 1229–1237 (2015).
8. S. W. Dickey, R. P. Baker, S. Cho, S. Urban, Proteolysis inside the membrane is a rate-governed reaction not driven by substrate affinity. *Cell* **155**, 1270–1281 (2013).
9. A. J. B. Kreutzberger, M. Ji, J. Aaron, L. Mihaljević, S. Urban, Rhomboid distorts lipids to break the viscosity-imposed speed limit of membrane diffusion. *Science* **363**, eaao0076 (2019).
10. A. N. Bondar, Mechanisms by which lipids influence conformational dynamics of the GlpG intramembrane protease. *J. Phys. Chem. B* **123**, 4159–4172 (2019).
11. M. K. Lemberg, K. Strisovsky, Maintenance of organellar protein homeostasis by ER-associated degradation and related mechanisms. *Mol. Cell* **81**, 2507–2519 (2021).
12. A. Ticha, B. Collis, K. Strisovsky, The rhomboid superfamily: Structural mechanisms and chemical biology opportunities. *Trends Biochem. Sci.* **43**, 726–739 (2018).

13. S. Urban, M. S. Wolfe, Reconstitution of intramembrane proteolysis in vitro reveals that pure rhomboid is sufficient for catalysis and specificity. *Proc. Natl. Acad. Sci. U.S.A.* **102**, 1883–1888 (2005).
14. J. A. Killian, Hydrophobic mismatch between proteins and lipids in membranes. *Biochim. Biophys. Acta* **1376**, 401–416 (1998).
15. M. R. de Planque, J. A. Killian, Protein-lipid interactions studied with designed transmembrane peptides: Role of hydrophobic matching and interfacial anchoring. *Mol. Membr. Biol.* **20**, 271–284 (2003).
16. O. Soubias, S. L. Niu, D. C. Mitchell, K. Gawrisch, Lipid-rhodopsin hydrophobic mismatch alters rhodopsin helical content. *J. Am. Chem. Soc.* **130**, 12465–12471 (2008).
17. E. Salnikov, C. Aisenbrey, B. Bechinger, Lipid saturation and head group composition have a pronounced influence on the membrane insertion equilibrium of amphipathic helical polypeptides. *Biochim. Biophys. Acta* **1864**, 183844 (2022).
18. M. K. Lemberg, J. Menendez, A. Misik, M. Garcia, C. M. Koth, M. Freeman, Mechanism of intramembrane proteolysis investigated with purified rhomboid proteases. *EMBO J.* **24**, 464–472 (2005).
19. S. Maegawa, K. Ito, Y. Akiyama, Proteolytic action of GlpG, a rhomboid protease in the Escherichia coli cytoplasmic membrane. *Biochemistry* **44**, 13543–13552 (2005).
20. P. Schmidt, B. J. Bender, A. Kaiser, K. Gulati, H. A. Scheidt, H. E. Hamm, J. Meiler, A. G. Beck-Sickinger, D. Huster, Improved in vitro folding of the Y2 G protein-coupled receptor into bicelles. *Front. Mol. Biosci.* **4**, 100 (2018).
21. H. I. Petrache, S. W. Dodd, M. F. Brown, Area per lipid and acyl length distributions in fluid phosphatidylcholines determined by ^{2}H NMR spectroscopy. *Biophys. J.* **79**, 3172–3192 (2000).
22. J. Schiller, M. Müller, B. Fuchs, K. Arnold, D. Huster, ^{31}P NMR Spectroscopy of phospholipids: From micelles to membranes. *Curr. Anal. Chem.* **3**, 283–301 (2007).
23. A. J. De Siervo, Alterations in the phospholipid composition of Escherichia coli B during growth at different temperatures. *J. Bacteriol.* **100**, 1342–1349 (1969).
24. U. Krug, A. Gloge, P. Schmidt, J. Becker-Baldus, F. Bernhard, A. Kaiser, C. Montag, M. Gauglitz, S. A. Vishnivetskiy, V. V. Gurevich, A. G. Beck-Sickinger, C. Glaubitz, D. Huster, The conformational equilibrium of the neuropeptide Y2 receptor in bilayer membranes. *Angew. Chem. Int. Ed.* **59**, 23854–23861 (2020).
25. A. Ticha, S. Stanchev, J. Škerle, J. Began, M. Ingr, K. Švehlová, L. Polovinkin, M. Růžička, L. Bednárová, R. Hadravová, E. Poláchová, P. Rampírová, J. Březinová, V. Kašička, P. Majer, K. Strisovsky, Sensitive versatile fluorogenic transmembrane peptide substrates for rhomboid intramembrane proteases. *J. Biol. Chem.* **292**, 2703–2713 (2017).
26. P. G. Scherer, J. Seelig, Electric charge effects on phospholipid headgroups. Phosphatidylcholine in mixtures with cationic and anionic amphiphiles. *Biochemistry* **28**, 7720–7728 (1989).
27. F. Lindström, P. T. Williamson, G. Gröbner, Molecular insight into the electrostatic membrane surface potential by 14n/31p MAS NMR spectroscopy: Nociceptin-lipid association. *J. Am. Chem. Soc.* **127**, 6610–6616 (2005).
28. D. Huster, Solid-state NMR spectroscopy to study protein-lipid interactions. *Biochim. Biophys. Acta* **1841**, 1146–1160 (2014).
29. Y. Wang, Y. Zhang, Y. Ha, Crystal structure of a rhomboid family intramembrane protease. *Nature* **444**, 179–180 (2006).
30. O. Soubias, W. E. Teague, K. G. Hines, K. Gawrisch, The role of membrane curvature elastic stress for function of rhodopsin-like G protein-coupled receptors. *Biochimie* **107**, 28–32 (2014).
31. E. Winkler, F. Kamp, J. Scheuring, A. Ebke, A. Fukumori, H. Steiner, Generation of Alzheimer disease-associated amyloid β42/43 peptide by γ-secretase can be inhibited directly by modulation of membrane thickness. *J. Biol. Chem.* **287**, 21326–21334 (2012).
32. K. Strisovsky, H. J. Sharpe, M. Freeman, Sequence-specific intramembrane proteolysis: Identification of a recognition motif in rhomboid substrates. *Mol. Cell* **36**, 1048–1059 (2009).
33. R. P. Baker, S. Urban, Architectural and thermodynamic principles underlying intramembrane protease function. *Nat. Chem. Biol.* **8**, 759–768 (2012).
34. E. J. Greenblatt, J. A. Olzmann, R. R. Kopito, Derlin-1 is a rhomboid pseudoprotease required for the dislocation of mutant α-1 antitrypsin from the endoplasmic reticulum. *Nat. Struct. Mol. Biol.* **18**, 1147–1152 (2011).
35. A. N. Bondar, C. del Val, S. H. White, Rhomboid protease dynamics and lipid interactions. *Structure* **17**, 395–405 (2009).
36. X. D. Wu, T. A. Rapoport, Translocation of proteins through a distorted lipid bilayer. *Trends Cell Biol.* **31**, 473–484 (2021).
37. A. M. Liaci, B. Steigenberger, P. C. T. de Souza, S. Tamara, M. Gröllers-Mulderij, P. Ogrissek, S. J. Marrink, R. A. Scheltema, F. Förster, Structure of the human signal peptidase complex reveals the determinants for signal peptide cleavage. *Mol. Cell* **81**, 3934–3948.e11 (2021).
38. H. E. Klock, S. A. Lesley, The polymerase incomplete primer extension (PIPE) method applied to high-throughput cloning and site-directed mutagenesis. *Methods Mol. Biol.* **498**, 91–103 (2009).
39. E. M. Pacull, F. Sendker, F. Bernhard, H. A. Scheidt, P. Schmidt, D. Huster, U. Krug, Integration of cell-free expression and solid-state NMR to investigate the dynamic properties of different sites of the growth hormone secretagogue receptor. *Front. Pharmacol.* **11**, 562113 (2020).
40. M. J. Hope, M. B. Bally, G. Webb, P. R. Cullis, Production of large unilamellar vesicles by a rapid extrusion procedure. Characterization of size distribution, trapped volume, and ability to maintain a membrane potential. *Biochim. Biophys. Acta* **812**, 55–65 (1985).
41. J. H. Davis, K. R. Jeffrey, M. Bloom, M. I. Valic, T. P. Higgs, Quadrupolar echo deuteron magnetic resonance spectroscopy in ordered hydrocarbon chains. *Chem. Phys. Lett.* **42**, 390–394 (1976).
42. M. Lafleur, B. Fine, E. Sternin, P. R. Cullis, M. Bloom, Smoothed orientational order profile of lipid bilayers by 2H-nuclear magnetic resonance. *Biophys. J.* **56**, 1037–1041 (1989).
43. D. Huster, K. Arnold, K. Gawrisch, Influence of docosahexaenoic acid and cholesterol on lateral lipid organization in phospholipid mixtures. *Biochemistry* **37**, 17299–17308 (1998).
44. T. Pott, E. J. Dufourc, Action of melittin on the DPPC-cholesterol liquid-ordered phase: A solid state 2H-and 31P-NMR study. *Biophys. J.* **68**, 965–977 (1995).
45. E. G. Bligh, W. J. Dyer, A rapid method of total lipid extraction and purification. *Can. J. Biochem. Physiol.* **37**, 911–917 (1959).

Acknowledgments: We would like to thank D. Langosch, H. Steiner, and F. Cichos for critical discussions on the manuscript. A. A. Smith-Penzel is acknowledged for help in preparing Fig. 4. **Funding:** This study was supported by Deutsche Forschungsgemeinschaft (DFG) grant 263531414 (to M.K.L. and D.H.). O.E. acknowledges financial support by the Sigrid Juselius Foundation, the Ruth and Nils-Erik Stenbäck's Foundation, and the Magnus Ehrnrooth Foundation. **Author contributions:** Conceptualization: D.H. and M.K.L. Methodology: D.U., M.K.L., and D.H. Investigation: O.E., D.U., V.D., A.P., V.S., and C.F. Visualization: O.E. and D.H. Supervision: D.H. and M.K.L. Writing—original draft: D.H. Writing—review and editing: O.E., D.U., V.D., V.S., C.F., A.P., M.K.L., and D.H. **Competing interests:** The authors declare that they have no competing interests. **Data and materials availability:** All data needed to evaluate the conclusions in the paper are present in the paper and/or the Supplementary Materials.

Submitted 3 May 2022
Accepted 9 August 2022
Published 23 September 2022
10.1126/sciadv.abq8303